Ceramics International xxx (xxxx) xxx

Contents lists available at ScienceDirect

Ceramics International

journal homepage: www.elsevier.com/locate/ceramint

Screen printed Zn-doped nanostructured In_2O_3 thick films, characterizations, and enhanced NO_2 gas sensing at low temperature

S.C. Kulkarni [a,*], Krishna D. Bhalerao [b], Sayantra Shirse [c], Yogesh T. Nakate [b,c], Umesh T. Nakate [d,**], Bidhan Pandit [e], M.A. Yewale [f]

[a] Department of Electronic Science, M. S. G. Arts, Science and Comm. College Malegaon-Camp (Nashik), Savitribai Phule Pune University, M.S, 423105, India
[b] School of Chemical Science, Department of Electronics, Kavayitri Bahinabai Chaudhari North Maharashtra University, Jalgaon, 425001, Maharashtra, India
[c] Department of Electronics, Yeshwant Mahavidyalaya Nanded, Nanded, Maharashtra, 423105, India
[d] Department of Polymer-Nano Science and Technology, Jeonbuk National University, 567 Baekje-daero, Deokjin-gu, Jeonju-si, Jeollabuk-do, Republic of Korea
[e] Department of Materials Science and Engineering and Chemical Engineering, Universidad Carlos III de Madrid, Avenida de la Universidad 30, 28911 Leganés, Madrid, Spain
[f] School of Mechanical Engineering, Yeungnam University, Gyeongsan, 38541, Republic of Korea

ARTICLE INFO

Keywords:
Nanostructured In_2O_3
Zn doping
NO_2 gas sensor
Selectivity
Low-temperature

ABSTRACT

The pristine and various mole% (1, 3, 5, 7, and 9) Zn-doped In_2O_3 nanocrystalline materials have been successfully prepared *via* the facile sol-gel and screen-printing thick film methods. The crystalline and morphological information for the samples were investigated using various techniques such as XRD, FESEM, HR-TEM, EDAX analysis, and AFM. All the fabricated sensor devices were employed to investigate sensing properties. The resistivity and activation energy properties of all samples were investigated. The 7 % mole Zn doped In_2O_3 sensor showed superior gas sensing properties and showed excellent selectivity towards NO_2 gas than other doped and pure In_2O_3 sensors. The sensors were tested at different operating temperatures for NO_2 gas. The highest response of 117 was revealed for 100 ppm NO_2 gas at 50 °C temperature. The optimal sensor device was tested for different NO_2 gas concentrations (50–500 ppm) and long-term stability (90 days). The plausible sensing mechanism was briefed. The Zn doped In_2O_3 materials could be a potential candidate for highly selective, low-temperature commercial NO_2 sensor device production.

1. Introduction

Various environmental issues such as acid rain, photochemical smog, ground-level ozone *etc.* are nothing but a result of nitrous oxide (NO_x) gas produced by thermal power plants, pulp mills, vehicles *etc*. NO_x is a corrosive and physiologically irritating gas; its long-term consumption can cause respiratory tract infection and lung diseases. Therefore, detection of this gas using high-performance sensors is of utmost importance.

Various types of sensors have been developed for NO_2 gas sensing, including electrochemical sensors, polymer sensors, surface acoustic waves sensors, metal oxide semiconductor (MOS) sensors [1–4] *etc*. to replace the heavy, expensive, and time-consuming analytical systems. Among these sensors, Metal Oxide Semiconductors (MOS) are popular due to their simplicity, small dimensions, good performance, and low cost. The widely used semiconductor oxides gas sensors such as SnO_2, ZnO, In_2O_3, and WO_3 are based on resistance change caused by the reaction between sensing materials and tested gases *via* the adsorption and desorption process. The gas-sensing performance mainly depends on crystallite size, surface morphology, composition, and microstructure [5,6].

Indium oxide (In_2O_3) is a very interesting semiconducting material that serves as an insulator in bulk form and behaves as a semiconductor with a direct optical band gap (3–4 eV) in its non-stoichiometric nano-size form. The In_2O_3 shows high transparency in the visible light range and is highly reflective in the IR light range. Novel applications can be investigated by synthesis of semiconductor nanostructures which depends on their structural properties like size and shape. It is reported that In_2O_3 shows high sensitivity to oxidizing gases *e.g.* NO_x [7], O_3 [8], as well as H_2. Yang et al. [9] prepared Zn-doped In_2O_3 nanocages and

* Corresponding author.
** Corresponding author.
E-mail addresses: sckulkarni12@gmail.com (S.C. Kulkarni), umesh.nakate@gmail.com (U.T. Nakate).

https://doi.org/10.1016/j.ceramint.2022.05.319
Received 24 April 2022; Received in revised form 18 May 2022; Accepted 25 May 2022
Available online 28 May 2022

hollow spindle-like nanostructure (HSNs) by hydrothermal method, and their results reveal that HSNs nanostructure exhibit higher and faster response than nanocages due to small particle size. Zhao and his co-workers [10] reported enhanced NO_2 gas sensing properties of In_2O_3 particles by doping them with Fe. Zhang et al. [11] studied Zn doped Indium oxide nanowires as transistors. Hu and co-workers [12] prepared Cu-doped hierarchical flowers like the In_2O_3 microsphere, and it shows highly enhanced NO_2 sensing performance. All above synthesis methods requires a high amount of energy [13] and cost and also able to produce pollutants, so there is a need for improvement. The use of nanostructured material has been preferred to produce highly sensitive gas sensors. The gas sensors based on nanostructured material and manufactured by thick film (screen printing) technology offer desirable advantages such as low cost, simplicity, and process reproducibility [14]. The sensitivity of the In_2O_3 sensor can be enhanced by doping it with various percentages of Zn.

In this paper, the unique nanostructured In_2O_3 sensor doped with different Zn mole % was fabricated on alumina using sol-gel and screen-printing techniques for highly selective and low-temperature NO_2 gas sensing applications with improved sensitivity. The prepared sensing materials were characterized using HR-TEM, FESEM, XRD, AFM, EDAX, *etc*. Detailed structural, morphological, and resistivity analyses were carried out. The activation energy for all doped sensors was investigated. All the sensors were tested for optimal operating temperature using NO_2 gas. The transient sensitivity and selectivity were studied for 100 ppm target gas. The effect of increasing NO_2 gas concentration and long-term stability were tested for 7 mole% Zn doped In_2O_3 sensor. The optimal NO_2 sensing performance was compared with reported data. The NO_2 gas sensing mechanism was presented for undoped and doped In_2O_3 sensors.

2. Experimental

2.1. Material synthesis

All purchased chemicals for the experiment were of analytical grade. Indium (III) Nitrate hydrate ($In(NO_3)_3.H_2O$, 99.9% purity Sigma Aldrich) was utilized as starting material, and Zinc nitrate hexahydrate ($Zn(NO_3)_2,6H_2O$ with purity 99 %, Merck) used as a dopant. The detailed synthesis process for pure In_2O_3 has been described in our previous publication [15]. In a typical In_2O_3 synthesis, 0.4 M Indium nitrate solution was prepared using 60 mL of DI water. After obtaining a clear solution, 0.4 M ammonia solution was added to the above-prepared solution till 9 pH dropwise with constant stirring. The precipitate was observed, and stirring continued for 30 min. The precipitate was washed and separated using centrifuge machines and solvents (DI water and methanol). The product was dried and annealed at 400 ^{0}C for 1 h.

The above synthesis process was adopted to prepare Zn doped In_2O_3 samples too. The appropriate molar concentration of Zinc nitrate hexahydrate ($(Zn(NO_3)_2{\cdot}6H_2O$, with purity 99 %, Merck) was added to the indium nitrate aqueous solution, and the rest of the process kept the same. A different zinc molar percentage prepared samples named as 1 %, 3 %, 5 %, 7 %, and 9 % of Zn in In_2O_3. These powder samples were utilized to fabricate thick films gas sensor devices.

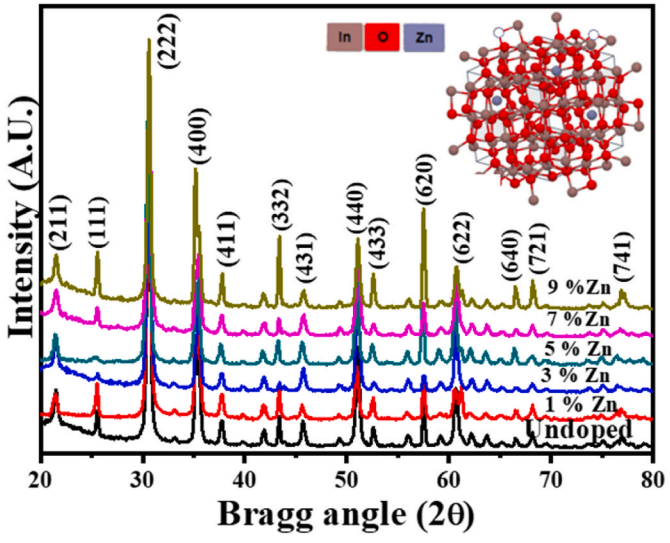

Fig. 1. XRD patterns of undoped and various mole% Zn doped In_2O_3 thick films on alumina substrate.

2.2. Fabrication of sensor

Thick films were fabricated using calcined powder by the screen-printing method. The paste (active sensor material) used for screen printing consists of two parts (i) solid phase and (ii) liquid phase. A ratio of 7:3 was taken for the solid and liquid phases, respectively. The solid phase is of active sensor material (powder and glass frit), whereas the liquid phase is of the organic vehicle, which is temporary binders. Calcined indium oxide powder was used as active materials along with 5 % (by weight) of locally prepared glass frit based on silicon composition (74, 13, 10.5, 1.3, 0.3, 0.2, 0.2 % = SiO_2, Na_2O, CaO, Al_2O_3, K_2O, SO_3, MgO). Ethylcellulose (EC, Aldrich) and Butyl Carbitol Acetate (BCA, Aldrich) were used as temporary binders. These binders are known to give thixotropic property to the paste. The paste for the thick film printing was prepared by finely grinding the calcined powder in agate-mortar and pestle. Then EC was added and well mixed with powder. Then BCA was added drop by drop and mixed well until the required viscosity was achieved [16], suitable for screen printing. The viscosity of the paste was controlled in a way that it passes easily through the screen and does smear on the substrate. The paste was then screen-printed (nylon mesh) onto alumina substrate (96 % pure, Kyocera). After screen printing, films dried using IR-lamp for 30 min to remove the organic vehicle, and then samples were fired at the optimized temperature (700 ^{0}C). The prepared thick film samples were investigated for gas sensing properties.

2.3. Structural and morphological characteristics

Information about the crystallinity and crystal phases of calcined powder and fired films were *via* X-ray diffraction (XRD, Bruker D8) technique with Cu kα radiation ($\lambda = 1.542$ A^0) for Bragg angles ranging from 20 to 80°. The morphology and chemical composition were examined by Field emission scanning electron microscope (FESEM model No-Zeiss Ultra 55 FESEM with oxford EDAX system). The surface topography, surface area, and surface roughness properties of undoped and Zn doped In_2O_3 films were studied with the help of atomic force microscopy (Asylum MFP 3D manufactured by Oxford Instruments Inc). The AFM analysis was carried out with non-contact mode in the ambient atmospheric condition and at room temperature. Scans area 1 μm × 1 μm was maintained. The surface area was measured using Gwyddion software.

2.4. Sensor characterization

The gas sensing characteristics (ppm level) were measured using a simple in-built static measuring system [17] under ambient atmospheric conditions, and the sensors were investigated for 100 ppm NO_2 gas concentrations. Gas sensing properties were studied as a function of different operating temperatures. To estimate the highest sensitivity, the sensor's operating temperature was raised from 50 to 300 ^{0}C in ambient and test gas (air and test gas mixture), by measuring the sensor's resistance as a function of temperature simultaneously. A change in sensor's resistance was recorded at different operating temperatures and the

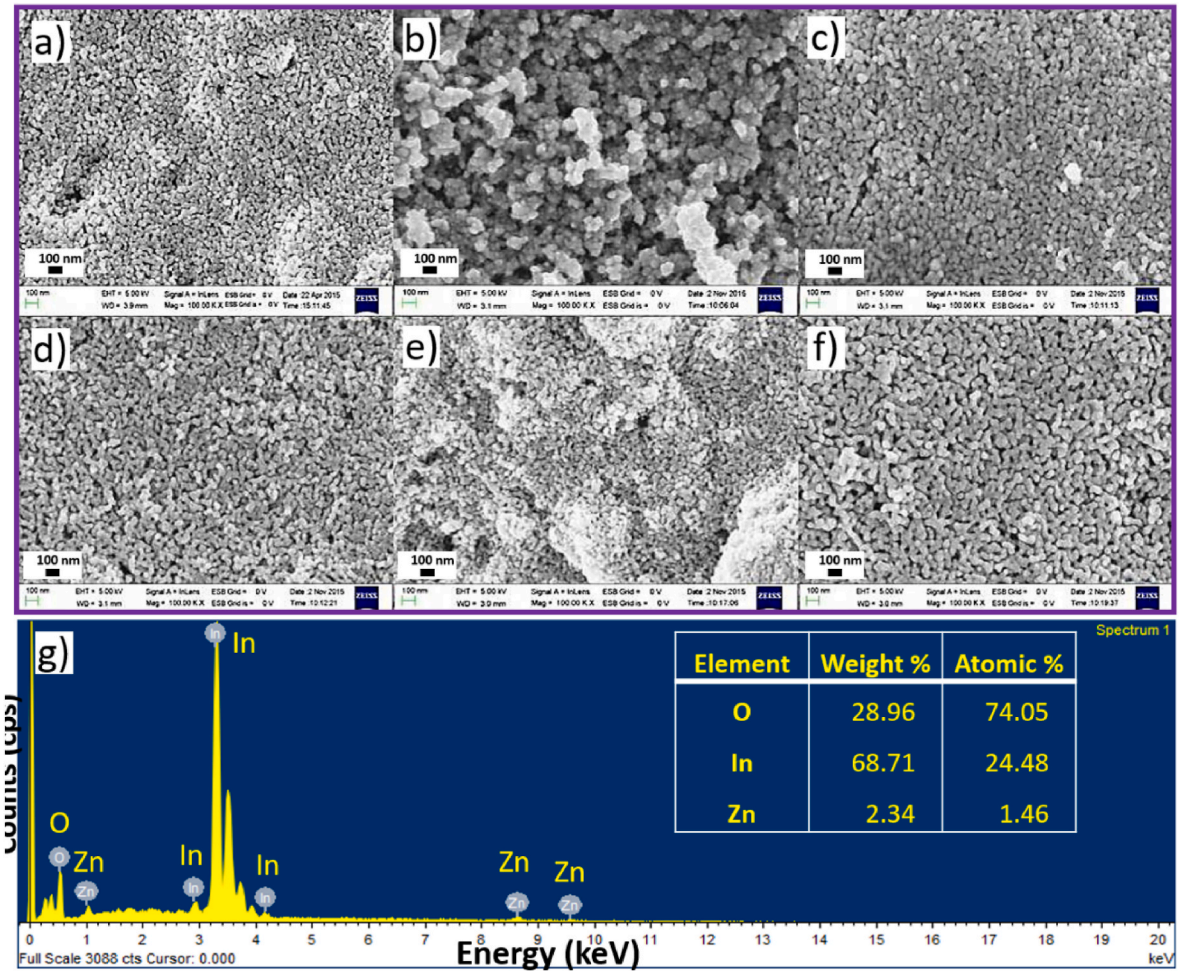

Fig. 2. FESEM images of (a) undoped, (b)1 mole%, (c) 3 mole%, (d) 5 mole %, (e) 7 mol%, (f) 9 mole%, Zn doped In_2O_3 thick films, (g) EDAX of 7 mole% doped In_2O_3 thick films (Inset shows elemental composition percentage).

relative difference in the resistance was taken as a measure of the gas sensing properties. The sensor's optimal temperature can be defined as the temperature at which the maximum change in the sensor's resistance is noted during the target gas exposure. In general, the optimal temperature can be varied depending on target gas. The sensitivity (S) of the sensor was defined as

$$S = \left|\frac{R_g}{R_a}\right| \quad (1)$$

where R_a and R_g are resistance values in air ambient and target gas plus air ambient, respectively, at the same operating temperature.

3. Results and discussion

3.1. Structural and morphological analysis

Fig. 1 shows the XRD pattern of undoped and Zn doped In_2O_3 thick film samples with different Zn concentrations (1, 3, 5, 7, and 9 mole %). All the samples exhibit a strong diffraction peak along (222) preferred orientation with additional low-intensity XRD peaks associated to (211), (400), (411), (431), (440), (620), and (622) planes, These XRD peaks were well matched with standard JCPDS card No.06-0416 confirming formation of cubic In_2O_3 compound. When Zn content increases, the lattice constant was found to decrease. The intensity of (222) peak increases with Zn doping. The high intensity in diffraction peaks in the XRD pattern suggests that samples are of high crystallinity.

The lattice constant of undoped and Zn doped In_2O_3 was calculated to know the influence of doped Zn ions. From XRD, the spacing between planes 'd' is related to lattice constant '*a*' for cubic structure and miller indices by the following equation.

$$a = \frac{\sqrt{3}}{sin\theta}\lambda \quad (2)$$

No additional peaks due to Zn was observed, whereas some observed peaks are due to alumina substrate [18].

It is evident from the lattice parameter calculation that there is a decrease in particle size with increasing Zn doping until 7 % and then suddenly increase to ~17.36 nm at 9 % doping. This indicates that during synthesis, Zn atoms are trying to replace Indium atoms in the lattice, which creates stress in the material. This is a clear indication that a mixed-phase has been synthesized with increasing Zn-doping, which could be detected in XRD observations. It is reported that about 6 % weight loss is observed in the case of pure In_2O_3 in the range above 250 to 800 °C, indicating that calcination is needed to stabilize the powder after synthesis. It can be seen from the XRD spectra that with increasing Zn-doping, a shift in peak positions was noticed. We believe that there could be two reasons for such a shift. Since the doping was done at a percentage level than the atomic level, a proper replacement with a lattice item might not have taken place and hence created strain in the material. This strain could be due to ionic radius of substituent ion Zn^{2+} (0.074 nm) which is smaller than the host ion In^{3+} (0.081 nm). The lattice distortion is due to various defects might lead to the XRD peak position shift that depends on the strain type *i.e.* tensile or compressive strain, the peak position shift respectively towards higher or lower

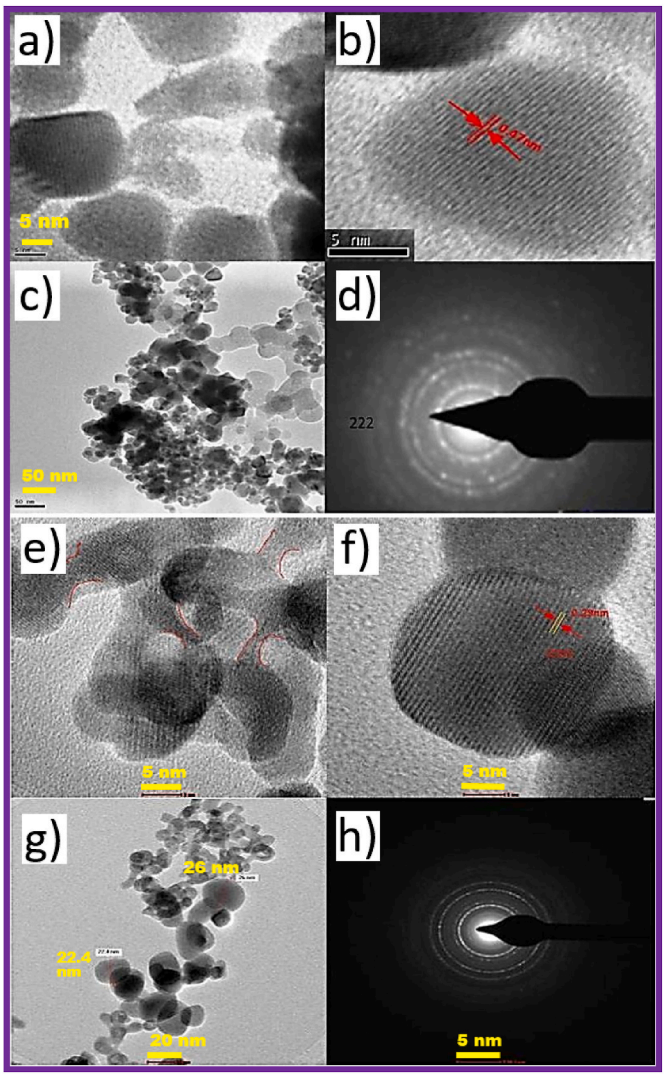

Fig. 3. a) – c) HR-TEM images, d) SAED pattern of In_2O_3 particles, and e) – g) HR-TEM images, h) SAED pattern of 7 mole% In_2O_3 particles.

angle. The other reason could be the mixed phase of the synthesized material at a higher doping percentage. It may happen that 7 % or 9 % sample may have phase separation, just like spinodal decomposition, where the maximum metastable solid solution decomposes into two phases. One of them may be a solid solution with a smaller concentration, so the peak may be shifted to a higher angle.

Fig. 2 (a) shows FESEM image of the undoped thick film, whereas Fig. 2(b), (c), (d), (e), and (f) depict FESEM images of 1, 3, 5, 7, and 9 mole% Zn doped In_2O_3 thick films, respectively. The composition of the thick film was analysed using EDAX data. The EDAX for 7 mole% Zn doped In_2O_3 thick films is shown in Fig. 2 (g), and the inset shows their elemental composition percentage. The EDAX for other Zn doped In_2O_3 thick films is shown in Fig. S1. The atomic percentages of all thick films samples are summarized in Table S1. It was observed from EDAX analysis that undoped In_2O_3 shows the presence of 'In' and 'O'. Whereas, various mole% Zn doped In_2O_3 samples show an increasing amount of Zn along with 'In' and 'O' elements.

Fig. 3 depicts the HR-TEM image and selected area electron diffraction (SAED) of calcined In_2O_3 nanocrystalline powder. The particles observed in HR-TEM image were irregular in shape, as represented in Fig. 3 (a) - (c). Fig. 3 (b) depicts HR-TEM image of In_2O_3 nanoparticles having perfectly crystalline particles in the form of a single crystal, exhibiting the lattice planes. The particle size was observed, which varied from 17 to 23 nm. The corresponding selected area diffraction pattern (SAED) of the In_2O_3 sample shows a spotty ring pattern without any additional diffraction spots and rings, revealing their crystalline cubic structure along (222) plane. The measured interplanar spacing d (hkl) from the selected area electron diffraction pattern (Fig. 3 (d)) exhibits (211), (222), (400), (411), (332), (431), and (440) planes that confirm cubic phase of In_2O_3 which is in good agreement with x-ray diffraction pattern (JCPDS card number 06–0416). The particles were mainly spherical and agglomerated.

In the case of 7 mole% Zn doped In_2O_3 nanocrystalline powder particle size decreases so that HRTEM images of the sample have been studied. Fig. 3(e) depicts HR-TEM image of 7 mole% Zn doped In_2O_3 nanoparticles confirming crystalline nature and shows lattice planes with an interplanar distance 0.294 Å as shown in Fig. 3(f). This corresponds to (222) plane. HRTEM image, as shown in Fig. 3(e), depicts neck formation. Fig. 3(g) depicts the TEM image of calcinated 7 mole% Zn doped In_2O_3 nanocrystalline powder particles, and Fig. 3(h) represents the SAED pattern. The SAED pattern shows spotty rings, which reveal polycrystalline structure.

3D AFM images of undoped and various mole% (1, 3, 5, 7, and 9 %) Zn doped In_2O_3 thick films are shown in Fig. 4. The Surface topography, growth, and surface roughness properties of the film were studied with the help of atomic force microscopy. The AFM analysis was performed (with non-contact mode) at ambient atmosphere over 1 × 1 μm scan area, with resolution 512 × 512 pixels. In_2O_3 showed rectangular and triangular grain growth on alumina substrate with rms surface roughness ~41.3 nm per micron. High roughness is due to the screen-printing technique. Table 1 shows lattice constant, particle size measured using AFM, and Surface area measured using Gwyddion software of undoped and Zn doped In_2O_3.

3.2. Electrical characterization of Zn doped In_2O_3 thick films

The electrical properties of In_2O_3 thick films were influenced mainly by the doping concentration of Zn. Doping upgrades the crystallinity of the film. The resistivity increases due to the generation of holes as some of In^{3+} in the lattice may be substituted by Zn^{2+} within the crystal lattice, the n-type conductive mechanism up to 3 mole%. The electrical resistivity of the film increases with an increase in Zn content up to 3 mole%. Similar results were obtained by Jothibas et al. [19] for Zn doped In_2O_3 thin films by spray pyrolysis technique. The replacement would distort the In_2O_3 lattice. This kind of lattice distortion would result in increased stress. A further increase of Zn content decrease resistivity value up to 7 mole%, and it again increases for Zn concentration 9 mole%. When Zn^{2+} substitute for In^{3+}, oxygen vacancies would be additionally generated in the In_2O_3 structure due to charge difference. The number of oxygen defects would create structural instability. Hence, if Zn content further increases, different structural defects like the interstitial solid solution of Zn could be developed in order to maintain the structure of the crystal lattice. An increase in resistivity at high doping concentration was reported by Franke et al. [20] for Sn doped In_2O_3.

3.2.1. Resistivity

Fig. 5(a) depicts the resistivity of Zn doped In_2O_3 as a function of Zn doping concentration. The magnitude of electrical resistivity observed for Zn doped In_2O_3 samples was found to be larger as compared with undoped In_2O_3 samples. The undoped In_2O_3 has one type of defect in particles, but the doped films have additional defects due to Zn doping in In_2O_3. The modification causes the formation of heterogeneous inter grain boundaries of Zn-In_2O_3. The increased barrier height of the intergranular region of doped In_2O_3 may be responsible for the increasing resistivity of films [21,22]. The presence of Zn in In_2O_3 affects grain growth and decreases carrier mobility due to carrier scattering at the grain boundaries [22]. This may lead to an increase in resistivity [23] of doped films. The resistance variation of Zn doped In_2O_3 thick

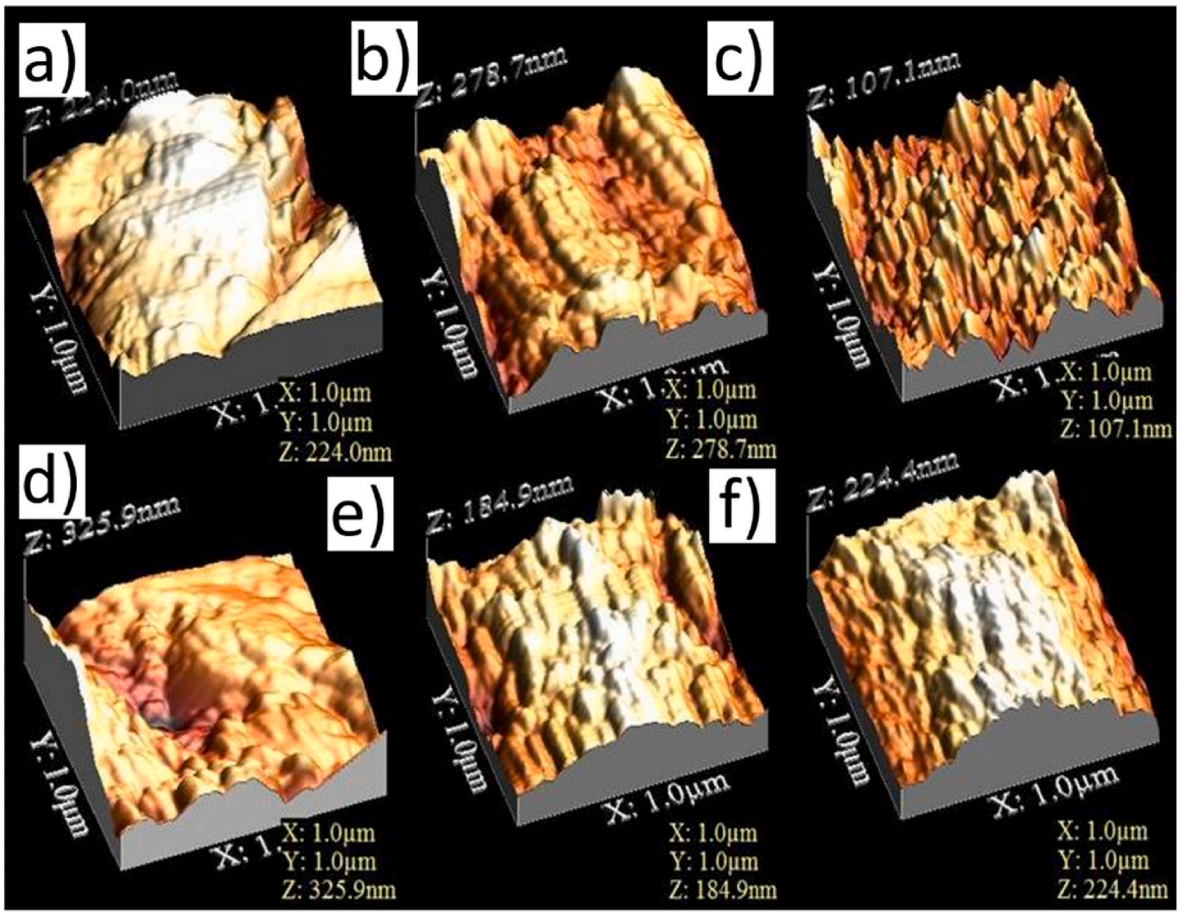

Fig. 4. AFM images of (a) undoped, (b)1 mole% Zn, (c) 3 mole% Zn, (d) 5 mole% Zn, (e) 7 mole% Zn (f) 9 mole% Zn doped In_2O_3 thick films on alumina substrate.

Table 1
Comparison of crystallite size, lattice constant, particle size, and surface area.

Material	Lattice Constant (Å)	Crystallite Size (nm)	Particle size (nm)	Surface area (μm^2)
Undoped In_2O_3	10.133	11.38	29	1.2462
1 % Zn doped	10.114	11.52	50	1.2399
3 % Zn doped	10.111	14.22	44	1.2415
5 % Zn doped	10.136	14.62	33	1.2421
7 % Zn doped	10.111	13.27	30	1.2516
9 % Zn doped	10.111	17.36	41	1.1908

films as a function of operating temperature shows semiconducting behaviour (*i.e.* resistance drop for increasing temperature) due to a negative temperature coefficient of resistance.

3.2.2. Activation energy

According to the Arrhenius graphs (Fig. 5 (b)–(f)), two distinct regions of temperatures (*i.e.* low and high-temperature regions) can be observed. In these graphs, the change in the slope of the graph occurs between two temperatures from one region to another. This depends on the doping concentrations. In the low-temperature regions, activation energy is less because small thermal energy is sufficient for the activation of the charge carrier to take part in the conduction process. For low-temperature regions, an electrical conductivity increased which may be

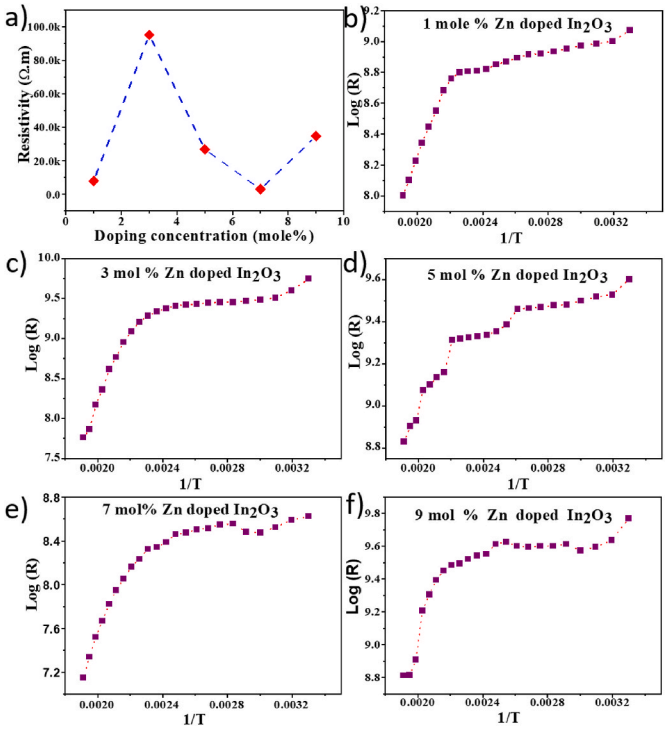

Fig. 5. a) Resistivity of the In_2O_3 thick films as a functi mole% doping, and Arrhenius plots for (b) 1 mole% (c) 3 mole% (d) 5 mole % (e) 7 mole% (f) 9 mole%, Zn doped In_2O_3 thick films.

Table 2
Variation of resistivity, activation energy, and TCR of Zn doped In_2O_3 thick films with firing temperature.

Mole% Zn Doping	TCR/^{0}K at constant Temp.	Resistivity Ω-m	Activation Energy(eV)	
			L.T. Region	H.T. Region
1 % Zn	0.00498	8.045E03	0.03019	0.60038
3 % Zn	0.00270	9.52E04	0.09468	0.96484
5 % Zn	0.00199	26.88E03	0.02935	0.71441
7 % Zn	0.00278	31.02E02	0.02446	0.73038
9 % Zn	0.00133	34.76E03	0.01736	0.98160

due to the charge carrier mobility, which depends on dislocation/defect concentrations. In high-temperature regions, activation energy is higher than in low-temperature regions. At higher temperatures, thermal fluctuations cause defects in crystal lattices. In this region, electrical conductivity is determined by intrinsic defects [24]. The activation energies are higher because of intrinsic defects. The variation of resistivity, activation energy, and temperature coefficient of resistance (TCR) of Zn doped In_2O_3 thick films with firing temperature is summarized in Table 2.

3.3. Sensor characterization

The gas sensing response is greatly influenced by the operating temperature because the adsorption and desorption process between tested gases and atmospheric oxygen O_2 for active surface sites are all regulated by temperature [25]. Therefore, responses to 100 ppm NO_2 for sensor-based on pure and 1, 3, 5, 7, 9, mole% Zn-doped thick films sensors were tested at a different operating temperature. The gas sensing responses of pure In_2O_3 and mole% Zn doped In_2O_3 sensors to the NO_2 gas at different operating temperatures were studied. Fig. 6(a) depicts a graph of variations in the sensitivity factor of all the sensors at different operating temperatures for 100 ppm NO_2 gas. The sensitivity factor increases with operating temperature and reaches the maximum value at 100 °C. This temperature is known as optimal temperature. It was observed that pure In_2O_3 sensors showed the highest sensitivity toward test gas at 100 °C. It can be observed from Fig. 6(a) that the sensitivities of all thick films varied dramatically with operating temperatures. As temperature increases, the activity of gas molecules and sensing material increases. The gas response was improved due to the use of Zn dopants. The thick films based on 7 mole% Zn doped In_2O_3 sensor exhibited the highest response at the lowest operating temperature *viz* 50 ^{0}C. The metal doping into semiconducting metal oxide gas sensor material often reveals the lower operating temperatures and higher response than pristine sensor. The high temperature would cause low diffusion length and which is responsible for the decreased response of the sensor [26].

The operating temperature of 7 mole% Zn-doped In_2O_3 sensor is low (50 °C) means low power consumption with high sensitivity and selectivity, which would be an excellent NO_2 sensor for practical applications. The study of the dynamic sensitivity of the sensor is quite important in order to use devices commercially. The transient (dynamic) sensitivity study for undoped and 7 mole% Zn doped In_2O_3 sensor was studied at 50 °C and represented in Fig. 6(b). The sensitivity of the sensors was increased as the target 100 ppm NO_2 gas was injected into the testing chamber, whereas sensitivity started falling down as the target gas was taken out. The rate of increase in response during target

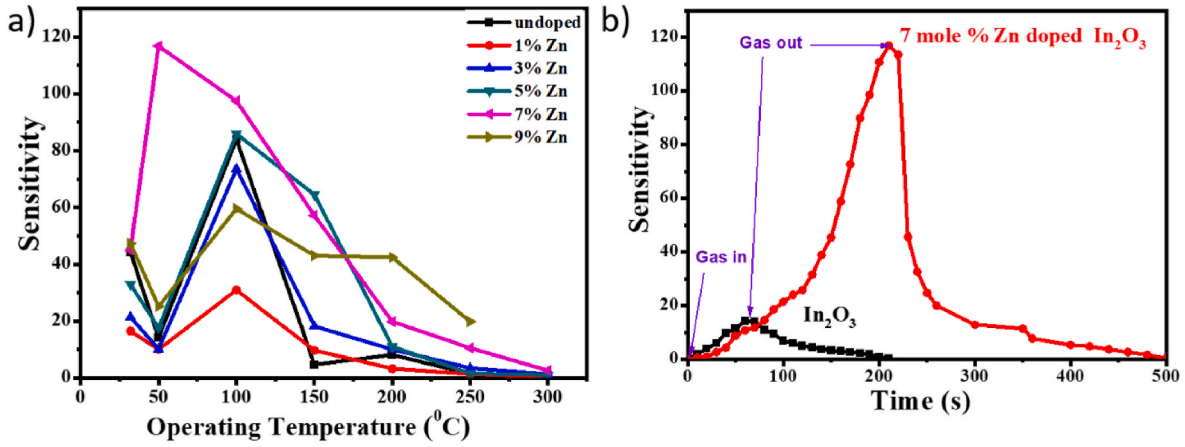

Fig. 6. (a) Sensitivity versus operating temperature for undoped and various mole% Zn doped In_2O_3 sensors for 100 ppm NO_2 gas. (b) Transient sensitivity for undoped and 7 mole% Zn doped In_2O_3 sensors for 100 ppm NO_2 gas at 50 °C.

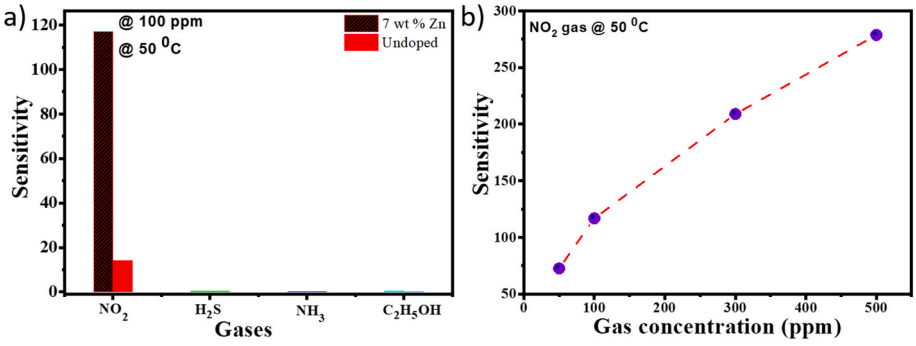

Fig. 7. (a) Selectivity study for undoped and 7 mole% Zn doped In_2O_3 sensors at 50 °C. (b) Sensitivity as a function of increasing NO_2 gas concentration at optimum temperature 50 °C.

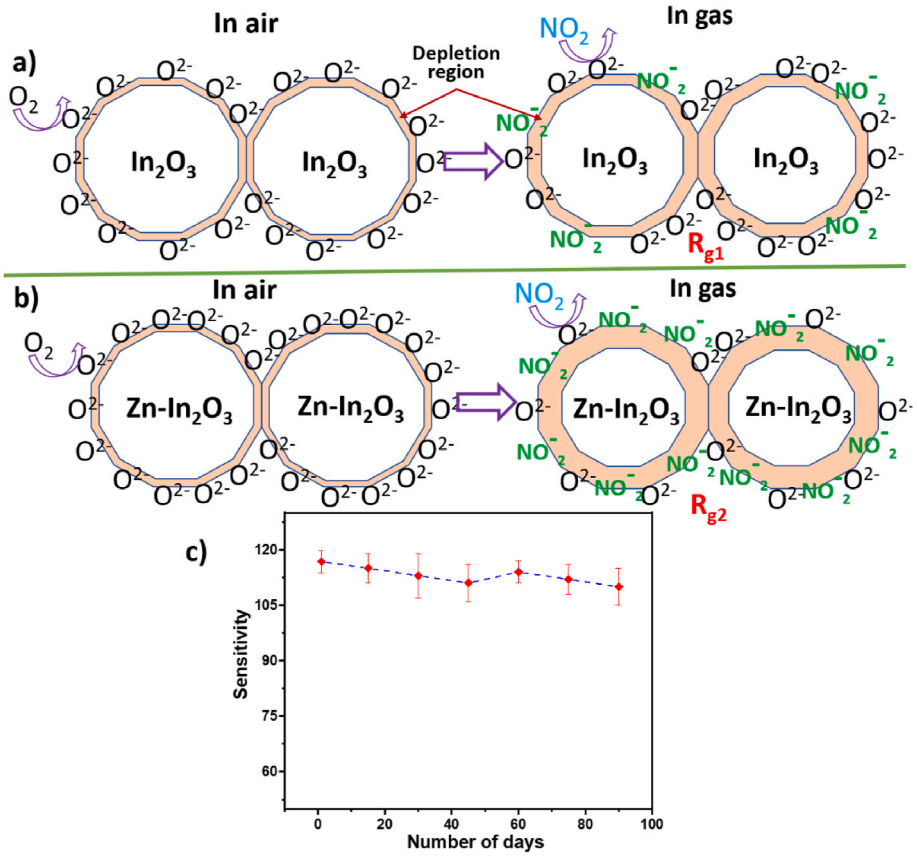

Fig. 8. Schematic mechanism of NO_2 gas sensing for (a) In_2O_3, (b) Zn-In_2O_3 sensors, (c) Stability study of 7 mole% Zn doped In_2O_3 sensor 100 ppm NO_2 gas at optimum temperature 50 °C.

gas exposure to sensor surface depends on several parameters such as diffusion coefficient of target gas in the carrier gas and air inside the testing chamber, adsorption properties of the sensor surface, speed of chemical catalytic sensing reaction, amount of target gas present in testing chamber *etc*. The doped sensor device revealed higher sensitivity than the undoped sample during transient gas sensing study.

The selectivity is also an essential parameter of gas sensors for practical applications. The selectivity of the sensor material towards particular gas depends on various parameters such as the chemical properties, crystal orientation, morphology, operating temperature, type of target gas *etc*. The selectivities of undoped and 7 mole% Zn-doped In_2O_3 sensors were evaluated by exposing sensors to different target gases at the optimal temperature of 50 °C for 100 ppm target gas. Fig. 7(a) shows the cross-sensitive response of the sensors to various gases, including H_2S, C_2H_5OH, and NH_3.

Both the sensors showed maximum response towards NO_2 gas (high selectivity) compared to other target gases at 50 °C. Whereas 7 mole% Zn-doped In_2O_3 sensor showed higher sensitivity (117) than undoped (14) sensor, thereby confirming higher selectivity. The optimal sensor *viz* 7 mole% Zn-doped In_2O_3 sensor showed higher sensitivity and selectivity at relatively low temperature. Hence, the only optimal sensor tested for further studies. Fig. 7(b) reveals the relationship between the sensitivity of 7 mole% Zn doped In_2O_3 sensor at increasing NO_2 concentrations (50–500 ppm) at an optimum temperature 50 °C. The sensor response was increased with an increase in NO_2 concentrations range. The increased sensitivity at higher concentrations is due to the number of target gas molecules adsorbed at sensor surface and chemically reacted, giving maximum change in sensor's resistance. The sensitivity of 72 and 278 were noted for 50 and 500 ppm NO_2 gas concentrations at 50 °C.

The NO_2 gas sensing mechanism can be described in two ways by following equation (3) to equation (5). In one mechanism, the NO_2 gas molecules adsorb at the sensor's surface directly, and it extracts electrons from the sensor surface (conduction band) [Eq. (3)], whereas, in the second mechanism, NO_2 gas molecules interact with the chemisorbed oxygen ions [Eq. (4) and Eq. (5)] [27].

$$NO_{2(gas)} + e^- \rightarrow NO^-_{2(ads)} \quad (3)$$

$$NO_{2(gas)} + O^-_{2(ads)} + 2\,e^- \rightarrow NO^-_{2(ads)} + 2\,O^-_{(ads)} \quad (4)$$

$$NO_{2(gas)} + O^-_{(ads)} \rightarrow NO^+_{(ads)} + 2\,O^-_{(ads)} \quad (5)$$

When Zn ions are doped into In_2O_3 crystals, some In^{3+} cations can be substituted by Zn^{2+}, and this substitution will be compensated by the generation of either holes or indium interstitials defects. The generated holes will recombine with electrons, which are the majority charge carriers in In_2O_3. Due to this, electron concentrations in the conduction band of In_2O_3 sensing material will be decreased, which causes an increase in resistance. equations (3)–(5) show that electrons are consumed in reactions that cause increased resistance of film during the NO_2 exposure. The schematics of the NO_2 sensing mechanism for undoped and Zn doped In_2O_3 sensors are shown in Fig. 8(a) and (b), respectively. The increase in the sensor's resistance (R_{g2}) rate is higher for the doped sensor than for the undoped sensor (R_{g1}). It was observed that sensitivity increases or decreases due to the adsorption and desorption phenomenon observed in gases [28]. The highest sensitivity factor is due to the smallest grain size within the film, as seen in FESEM of 7 mole% Zn doped In_2O_3.

The stability of the sensor element was measured for 100 ppm concentrations of NO_2 by repeating the test for up to three months from the first measurement at 50 °C. The results are shown in Fig. 8 (c). There is very little variation in sensitivity along with error bar was noted during stability test, indicating the excellent stability of the sensor. There are

Table 3
A comparison between the NO_2 sensing characteristics of the present sensors and those reported in the literature.

Material	NO_2 Conc. (ppm)	Optimal Temp. (^{0}C)	Sensitivity /Response	References
In_2O_3	0.7	250	10	[29]
In_2O_3 nanoribbon	5	200	70	[30]
In_2O_3 nanowires	1	250	2.57	[31]
In_2O_3:SnO_2	250	250	7.5	[32]
In_2O_3:Gd_2O_3	100	195	79	[33]
In_2O_3 microsphere	5	250	1.5	[34]
In_2O_3: MoO_3:	1	250	23	[35]
In_2O_3: Au	10	350	14.26	[36]
In_2O_3	**100**	**100**	**84**	**Present work**
Zn: In_2O_3	**100**	**50**	**116.8**	**Present work**

reports available on different sensor materials for NO_2 gas sensing application. A comparison between the sensing performance of 7 mole% Zn doped In_2O_3 sensor and reported in the literature was carried out and summarized in Table 3. As observed from the table, the sensor presented in the current work exhibits better sensing performance at low operating temperatures than reported in the literature [29–36].

The 7 mole% Zn doped In_2O_3 exhibit excellent response at low operating temperature (50 °C), which means low power consumption and good selectivity shed light on a new promising candidate for atmospheric pollution monitoring and practical applications.

4. Conclusions

The nanocrystalline pure In_2O_3 and Zn-doped (1, 3, 5, 7, and 9 %) In_2O_3 powders were synthesized using the facile sol-gel route and were fabricated on alumina substrate using a standard screen-printing technique. The HR-TEM and FESEM demonstrated the small particle size observed for 7 mole% Zn-doped In_2O_3 thick films. Detail structural, resisitivity, and activation energy studies were carried out systematically. Effects of Zn doping on structural and gas sensing properties of In_2O_3 sensor were studied. The 7 mole% Zn-doped In_2O_3 thick films show the highest sensitivity of 117 and selectivity towards 100 ppm NO_2 gas at a low temperature of 50 °C than other doped and pure In_2O_3 sensors. The plausible NO_2 sensing mechanisms were proposed. The performance of the present optimal sensor was observed to be highest among reported sensor's data. Such a sensor would require less power consumption due to low operating temperature. The long-term stability and dynamic sensitivity of the present Zn doped nanostructured In_2O_3 sensor could be a potential candidate for commercial NO_2 gas sensor devices for environmental monitoring applications.

Declaration of competing interest

The authors declare that they have no known competing financial interests or personal relationships that could have appeared to influence the work reported in this paper.

Acknowledgment

The authors are thankful to CEN, IITB for providing the necessary characterization facilities. One of the authors (SCK) acknowledges UGC New Delhi for the teacher fellowship under XII plan (file no. 34-25/13). She also acknowledges the Management of M.G. Vidyamandir and the principal of S.P.H. Mahila Mahavidyalaya Malegaon-Camp (Nashik), India for their support.

Appendix A. Supplementary data

Supplementary data to this article can be found online at https://doi.org/10.1016/j.ceramint.2022.05.319.

References

[1] J.S. Do, R.Y. Shieh, Electrochemical nitrogen dioxide gas sensor based on solid polymeric electrolyte, Sens. Actuators, A B37 (1996) 19–26.
[2] U.V. Patil, N.S. Ramgir, N. Karmakar, A. Bhogale, A.K. Debnatha, D.K. Aswal, S. K. Gupta, D.C. Kothari, Room temperature ammonia sensor based on copper nanoparticle intercalated polyaniline nanocomposite thin films, Appl. Surf. Sci. 339 (2015) 69–74.
[3] M.C. Horrillo, M.J. Fernandez, J.L. Fontecha, et al., Optimization of SAW sensor with a structure ZnO-SiO_2-Si to detect volatile organic compounds, Sens. Actuators, B 118 (2006) 356–361.
[4] Y. Wang, G. Duan, Y. Zhu, H. Zhang, Z. Xu, Z. Dai, W. Cai, Room temperature H2S gas sensing properties of In_2O_3 micro/nano structured porous thin film and hydrolyzation-inducedenhanced sensing mechanism, Sens. Actuators, B 228 (2016) 74–84.
[5] N. Barsan, D. Koziej, U. Weimar, Metal oxide-based gas sensor research: how to? Sens. Actuators, B 121 (2007) 18–35.
[6] N. Yamazoe, G. Sakai, K. Shimanoe, Oxide semiconductor gas sensors, Catal. Surv. Asia 7 (2003) 63–75.
[7] A. Gurlo, N. Barsan, M. Ivanovskaya, U. Weimar, W. Gopel, In_2O_3 and MoO_3–In_2O_3 thin film semiconductor sensors:interaction with NO_2 and O_3, Sens. Actuators, B 4 (1998) 92–99.
[8] M. Ivanovskaya, A. Gurlo, P. Bogdanov, Mechnism of O_3 and NO_2 detectation and selectivity of In_2O_3 sensor, Sens. Actuators, B 77 (1–2) (2001) 264–267.
[9] H. Yang, S. Wang, Y. Yang, Zn-doped In_2O_3 nanostructures: preparation, structure and gas-sensing properties, CrystEngComm 14 (2012) 1135–1142.
[10] J. Zhao, T. Yang, Y. Liu, Z. Wang, X. Li, Y. Sun, Y. Du, Y. Li, G. Lu, Enhancement of NO_2 gas sensing response based on ordered mesoporous Fe-doped In_2O_3, Sens. Actuators, A B191 (2014) 806–812.
[11] W.F. Zhang, Z.B. He, G.D. Yuan, J.S. Jie, L.B. Luo, X.J. Zhang, Z.H. Chen, C.S. Lee, W.J. Zhang, S.T. Lee, High-performance, fully transparent, and flexible zinc-doped indium oxide nanowire transistors, Appl. Phys. Lett. 94 (2009), 123103-3.
[12] X. Hu, L. Tian, H. Sun, B. Wang, Y. Gao, P. Sun, F. Liu, G. Lu, Highly enhanced No_2 sensing performances of Cu-doped In_2O_3 hierarchical flowers, Sens. Actuators, B 221 (2015) 297–304.
[13] N. Singh, C. Yan, P.S. Lee, Room temperature Co gas sensing using Zn-doped In_2O_3 single nanowires field effect transistor, Sens. Actuators, B 150 (2010) 19–24.
[14] A. Srivastava, S.T. Lakshmikumar, A.K. Srivastava, Rashmi, K. Jain, Gas sensing properties of nanocrystalline SnO_2 prepared in solvent media using a microwave assisted technique, Sens. Actuators, A B126 (2007) 583–587.
[15] S.C. Kulkarni, C.S. Aher, R.Y. Borse, B.G. Bharate, S.S. Al-Deyab, S.G. Ansari, P. K. Khanna, Gas sensing properties of nanocrystalline indium oxide synthesized by sol–gel method, *Adv. Sci. Lett.* 5no. 1 (2012) 109–113.
[16] S.C. Kulkarni, D.S. Patil, Effect of $PdCl_2$ molarity on the gas sensing properties of nanocrystalline indium oxide, Sens. Lett. 13 (4) (2015) 294–299.
[17] M.H. Madhusudan Reddy, A.N. Chandorkar, Response study of electron-beam evaporated thin-film tin oxide gas sensors, Sensor. Actuator. B 9 (1992) 1–8.
[18] Z.A. Ansari, S.G. Ansari, T. Ko, J.H. Oh, Effect of MoO_3 doping and grain size on SnO_2. enhancement of sensitivity and selectivity for CO and H_2 gas sensing, Sens. Actuators, B 87 (1) (2002) 105–114.
[19] M. Jothibas, C. Manoharan, S. Ramalingam, S. Dhanapandian, M. Bououdina, Spectrochim. Acta Mol. Biomol. Spectrosc. 122 (2014) 171–178.
[20] M.E. Franke, T.J. Koplin, U. Simon, Metal and metal oxide nanoparticles in chemiresistors: does the nanoscale matter? Small 2 (1) (2006) 36–50.
[21] D.R. Patil, L.A. Patil, P.P. Patil, Cr_2O_3-activated ZnO thick film resistors for ammonia gas sensing operable at room temperature, Sens. Actuators, B 126 (2) (2007) 368–374.
[22] D.R. Patil, L.A. Patil, Cr_2O_3-modified ZnO thick film resistors as LPG sensors, Talanta 77 (4) (2009) 1409–1414.
[23] K. Tominaga, T. Takao, A. Fukushima, T. Moriga, I. Nakabayashi, Film properties of ZnO: Al films deposited by co-sputtering of ZnO: Al and contaminated Zn targets with Co, Mn and Cr, Vacuum 66 (3) (2002) 511–515.
[24] I.S.A. Frag, I.K. Battisha, M.M.E. Rafaay, Study of dielectric properties of α-alumina doped with MnO, CdO and MoO, Indian J. Pure Appl. Phys. 43 (2005) 446–450.
[25] X. Tan, L. Sun, Z. Li, Y. Zhao, Side-by-side in$(OH)_3$ and In_2O_3 nanotubes synthesis and optical properties, Nanoscale Res. Lett. 5 (2010) 383–388.
[26] Q. Wan, T.H. Wang, Single-crystalline Sb-doped SnO_2 nanowires: synthesis and gas sensor applications, Chem. Commun. 384 (2005) 3841–3843.
[27] A. Gurlo, M. Ivanovskaya, N. Barsan, M. Schweizer-Berberich, U. Weimar, W. Gopel, A. Dieguez, Grain size control in nanocrystalline In_2O_3 semiconductor gas sensors, Sens. Actuators, B 44 (1997) 327–333.
[28] C.M. Ghimbeu, M. Lumbreras, M. Siadat, J. Schoonmam, Detection of Pollutant gases using electrostatic sprayed indium oxide and tin doped indium oxide, Mater. Chem. Phys. 114 (2009) 933–938.
[29] C. Cantalini, W. Wlodarski, H. Sun, M.Z. Atashbar, M. Passacantando, S. Santucci, NO_2 response of In_2O_3 thin film gas sensors prepared by sol–gel and vacuum thermal evaporation techniques, Sens. Actuators, B 65 (2000) 101–104.

[30] P.S. Khiabani, E. Marzbanrad, C. Zamani, R. Riahifar, B. Raissi, Fabrication of In_2O_3 based NO_2 gas sensor through AC-electrophoretic deposition, Sens. Actuators, A B166–167 (2012) 128–134.

[31] P. Xu, Z. Cheng, Q. Pan, J. Xu, Q. Xiang, W. Yu, Y. Chu, High aspect ratio In_2O_3 nanowires: synthesis, mechanism and NO_2 gas-sensing properties, Sens. Actuators, B 130 (2008) 802–808.

[32] G. Sberveglieri, S. Groppelli, G. Coccoli, Radio frequency magnetron sputtering growth and characterization of indium-tin oxide (ITO) thin films for NO_2 gas sensors, Sens. Actuators, B 15 (3) (1988) 235–242.

[33] X. Niu, H. Zhong, X. Wang, K. Jiang, Sensing properties of rare earth oxide doped In_2O_3 by a sol–gel method, Sensor. Actuator. B 115 (1) (2006) 434–438.

[34] Z. Cheng, L. Song, X. Ren, Q. Zheng, J. Xu, Novel lotus root slice-like self-assembled In_2O_3 microspheres: synthesis and NO_2-sensing properties, Sens. Actuators, B 176 (2013) 258–263.

[35] A. Gurlo, N. Barsan, M. Ivanovskaya, U. Weimar, W. Göpel, In_2O_3 and MoO_3–In_2O_3 thin film semiconductor sensors: interaction with NO_2 and O_3, Sens. Actuators, B 47 (1) (1998) 92–99.

[36] H. Steffes, C. Imawan, F. Solzbacher, E. Obermeier, Enhancement of NO_2 sensing properties of In_2O_3-based thin films using an Au or Ti surface modification, Sensor. Actuator. B Chem. 78 (2001) 106–112.